Constraints on Asian ozone using Aura TES, OMI and Terra MOPITT

Zhe Jiang[1], John. R. Worden[1], Dylan B. A. Jones[2,3], Jintai Lin[4], Willem W. Verstraeten[5,6], Daven K. Henze[7]

[1]Jet Propulsion Laboratory, California Institute of Technology, Pasadena, CA, USA
[2]Department of Physics, University of Toronto, Toronto, ON, Canada
[3]JIFRESSE, University of California, Los Angeles, Los Angeles, CA, USA
[4]Laboratory for Climate and Ocean-Atmosphere Studies, Department of Atmospheric and Oceanic Sciences, School of Physics, Peking University, Beijing, China
[5]Meteorology and Air Quality Department, Wageningen University, the Netherlands
[6]Earth Observation Climate Department, Royal Netherlands Meteorological Institute, the Netherlands
[7]Department of Mechanical Engineering, University of Colorado, Boulder, CO, USA

Abstract

Rapid industrialization in Asia in the last two decades has resulted in a significant increase in Asian ozone (O_3) pre-cursor emissions with likely a corresponding increase in the export of O_3 and its pre-cursors. However, the relationship between this increasing O_3, the chemical environment, O_3 production efficiency, and the partitioning between anthropogenic and natural precursors is unclear. In this work, we use satellite measurements of O_3, CO and NO_2 from TES (Tropospheric Emission Spectrometer), MOPITT (Measurement of Pollution In The Troposphere) and OMI (Ozone Monitoring Instrument) to quantify O_3 pre-cursor emissions for 2006 and their impact on free-tropospheric O_3 over North-East Asia, where pollution is typically exported globally due to strong westerlies. Using the GEOS-Chem global chemical transport model, we test the modeled seasonal and interannual variation of O_3 based on prior and updated O_3 pre-cursor emissions where the updated emissions of CO and NO_x are based on satellite measurements of CO and NO_2. We show that the observed TES O_3 variability and amount are consistent with the model for these updated emissions. However, there is little difference in the modeled ozone between the updated and prior emissions. For example, for the 2006 June time period, the prior and posterior NOx emissions were 14% different over China but the modeled ozone in the free-troposphere was only 2.5% different. Using the adjoint of GEOS-Chem we partition the relative contributions of natural and anthropogenic sources to free troposphere O_3 in this region. We find that the influence of lightning NO_x in the summer is comparable to the contribution from surface emissions but smaller for other seasons. China is the primary contributor of anthropogenic CO, emissions and their export during the summer. While the posterior CO emissions improved the comparison between model and TES by 32%, on average, this change also had only a small effect on the free-tropospheric ozone. Our results show that the

50 influence of India and Southeast Asia emissions on O_3 pollution export to the Northwest Pacific
51 is sizeable, comparable with Chinese emisisons in winter, about 50% of Chinese emissions in
52 spring and fall, and approximately 20% in the summer.
53

54 # 1. Introduction

55 Unprecedented growth in transportation, coal-fired power plants and the industrial sector
56 in China has resulted in a substantial increase in the emissions of O_3 precursors (Lin et al. 2014a).
57 Recent studies (Lamsal et al. 2011; Lin 2012; Mijling et al. 2013) show 5-10% annual growth
58 rate of NO_x emission in China. Wang et al. (2012) found there was 3% annual growth rate of O_3
59 in Beijing in the period of 2003-2010. East Asian O_3 can be transported to the surface of North
60 America in about 2-3 weeks (Liu and Mauzerall 2005) by midlatitude westerly winds (Liang et
61 al 2004, 2005), which likely results in an increase of background O_3 concentration in western
62 North America by 3-7 ppbv during the period of 2000 - 2006 (Zhang et al. 2008; Brown et al.
63 2011).

64 Use of inverse (top-down) methods to better quantify the emission of NO_x (Lamsal et al.
65 2011; Lin and McElroy 2011; Lin 2012; Mijling et al. 2013), VOCs (Shim et al. 2005; Fu et al.
66 2007) and CO (Kopacz et al. 2010; Fortems-Cheiney et al. 2011; Gonzi et al. 2011) are needed to
67 ensure consistency between bottom-up inventories and observations. However, large
68 discrepancies can still exist between bottom-up and top-down based inventories (e.g., Kopacz et
69 al., 2010, Lin et al. 2012b). In this work, we perform a multi-tracer assimilation with the GEOS-
70 Chem model to evaluate the top-down estimates of O_3 precursors (NO_x and CO) in East Asia.
71 We firstly optimized the CO and NO_x emission with MOPITT CO and OMI NO_2 retrievals
72 respectively and then evaluate the a posteriori simulation of CO and O_3 by comparing the values

with measurements from TES in the period of Dec 2005 – Nov 2006. Using the adjoint of the GEOS-Chem model (Henze et al., 2007), we then quantify source contributions (NO_x, CO, VOC) to free tropospheric O_3 pollution over East China and the China outflow region in Dec 2005 – Nov 2006.

2. Observations and Model

2.1. TES CO and O_3

The TES instrument was launched on NASA's Aura spacecraft on 15 July 2004. The satellite is in a sun-synchronous polar orbit of 705 km and crosses the equator at 1:45 and 13:45 local time. With a footprint of 8km x 5km, TES measures radiances between 3.3-15.4μm with global coverage of 16 days (Beer et al. 2001) of observations. In the troposphere, TES O_3 profile retrievals have 1-2 degrees of freedom for signal (DOFS), and about 1 DOFS for CO. We use data from the "lite" product (http://tes.jpl.nasa.gov/data/) which reports volume mixing ratios (VMR) on 26 pressure levels for O_3 and 14 pressure levels for CO. Using an optimal estimation approach, the TES retrievals are conducted with respect to the logarithm of the VMR. The relationship between the retrieved profiles and the true atmospheric state can be expressed as:

$$\hat{\mathbf{z}}^{TES} = \mathbf{z}_a^{TES} + \mathbf{A}^{TES}(\mathbf{z} - \mathbf{z}_a^{TES}) + \mathbf{G}\varepsilon \quad (1)$$

where $\mathbf{z}$ is the true atmospheric state (expressed as log(VMR)), $\mathbf{z}_a^{TES}$ is the TES a priori O_3 or CO profile, $\mathbf{A}^{TES}$ is the TES averaging kernel matrix and $\mathbf{G}\varepsilon$ describes the retrieval error. The averaging kernel matrix represents the sensitivity of the retrieval to the actual trace gas in the atmosphere. The TES retrievals use a monthly mean profile of the trace gas from the MOZART-4 CTM (chemical transport model), averaged over a 10º latitude x 60º longitude, as the a priori information $\mathbf{z}_a^{TES}$. According to the recommended quality control criterion, we only

use CO and O_3 data with major quality flag equals 1. These data have passed all major quality flags used to assess the TES data related to chi-2 tests, biases in the radiance residuals, and residual non-linearity checks. The data with small DOFS (Degree of Freedom for Signal for CO is smaller than 0.8), are dropped as the limited sensitivity reduces the robustness of calculated O_3-CO correlations. We empirically find that the sensitivity of CO is the limiting factor in these comparisons, that is, if DOFS of CO is > 0.8 then the DOFS of O_3 is > 0.8. Recently, Verstraeten et al. (2013) evaluated TES O_3 measurement by using data from World Ozone and Ultra-violet Radiation Data Centre (WOUDC) sites and found that there is a ~7 ppb bias in the TES measurements in free troposphere, and the magnitude is slightly larger in summer and smaller in winter. TES CO measurements were evaluated by Luo et al. (2007) using the aircraft measurents from INTEX-B campaingn. They showed that TES CO VMR profiles are 0-10% lower than the aircraft measurements in the lower and middle troposphere.

2.2. MOPITT CO

The MOPITT instrument was launched on NASA's Terra spacecraft on 18 December 1999. The satellite is in a sun-synchronous polar orbit of 705 km and crosses the equator at 10:30 local time. With a footprint of 22km x 22km, MOPITT (version 6) combines TIR (4.7μm) with the NIR (2.3μm) and has better sensitivity to lower tropospheric CO over land (Worden et al. 2010). MOPITT CO retrievals are reported on 10 pressure levels (surface, 900, 800, 700, 600, 500, 400, 300, 200 and 100 hPa). Similar to the TES product, relationship between the retrieved CO profiles and the true atmospheric state can be expressed as:

$$\hat{\mathbf{z}}^{MOP} = \mathbf{z}_a^{MOP} + \mathbf{A}^{MOP}(\mathbf{z} - \mathbf{z}_a^{MOP}) + \mathbf{G}\varepsilon \quad (2)$$

where $\mathbf{z}$ is the true atmospheric state (expressed as log(VMR)), $\mathbf{z}_a^{MOP}$ is the MOPITT a priori CO

117 profile, $\mathbf{A}^{MOP}$ is the MOPITT averaging kernel matrix and $\mathbf{G}\varepsilon$ describes the retrieval error.
118 Same as TES, the a priori information of MOPITT retrievals is from monthly mean profile of the
119 MOZART-4 CTM, without the 10º latitude x 60º longitude average. We reject MOPITT data
120 with CO column amounts less than $5x10^{17}$ molec/cm^2 and if low clouds are observed. The
121 nighttime data is excluded in the assimilation, due to the NIR radiances measure reflected solar
122 radiation. The version 5 data have been evaluated recently against NOAA aircraft measurements
123 (Deeter et al., 2013), which shows small bias in the low and middle troposphere, but 14%
124 positive bias at 200 hPa retrieval level. The new version 6 data significantly reduces the bias in
125 the upper troposphere but magnifies the positive bias at the surface level. In this work, we decide
126 to use the new version 6 data, as we focus on the free troposphere (above 800 hPa), which is not
127 affected by the positive bias in the retrieval at the surface level.

128 **2.3. OMI NO_2**

129 The OMI instrument was also launched on NASA's Aura spacecraft. The sensor has a
130 spatial resolution of 13 km x 24 km (Levelt et al. 2006). OMI provides daily global coverage
131 with measurements of both direct and atmosphere-backscattered sunlight in the ultraviolet-
132 visible range from 270 to 500 nm; 405-465 nm is used to retrieve tropospheric NO_2 columns. In
133 this study, the daily level-2 data from KNMI DOMINO-2 product (Boersma et al. 2011) are
134 averaged to obtain monthly mean vertical column densities (VCDs) for subsequent emission
135 inversion. The total error for the retrievaled VCDs is about 30% plus $0.7x10^{15}$ molec/cm$_2$, and
136 the magnitude is larger in winter than in summer (Boersma et al. 2011, Lin and McElroy 2011).
137 The pixels with cloud radiance fraction exceeding 50% are removed. In order to have a better
138 analysis of the spatial distribution of VCDs within short distance, we only uses data from the 30
139 pixels around the swath center. The details for the data treatment are described in Lin (2012).

2.4. GEOS-Chem

The GEOS-Chem CTM (http://www.geos-chem.org) is driven by assimilated meteorological observation from the NASA Goddard Earth Observing System (GEOS-5) at the Global Modeling and data Assimilation Office. We use version v34 of the GEOS-Chem adjoint, which is based on v8-02-01 of GEOS-Chem, with relevant updates through v9-01-01. The standard GEOS-Chem chemistry mechanism includes 43 tracers, which can simulate detailed tropospheric O_3-NO_x-hydrocarbon chemistry, including the radiative and heterogeneous effects of aerosols. The GEOS-5 meteorological fields have 72 vertical levels and the lowest 31 levels are terrain following levels. In order to minimize the amount of memory required to run GEOS–Chem, the model is run with a reduced vertical resolution, in which the levels in the stratosphere are lumped together online.

The native horizontal resolution of GEOS-5 is 0.5º x 0.667º, but it is usually degraded to 4°x5° or 2°x2.5° in global scale simulations. A nested simulation can be achieved by running a 0.5º x 0.667º resolution model within a regional domain using the boundary condition provided from a global, coarse resolution mode (Wang et al. 2004; Chen et al. 2009). Recently, the adjoint of nested GEOS-Chem was developed by Jiang et al. (2014). In this work, following Jiang et al. (2014) and Mao et al. (2014), we run the model with 0.5º x 0.667º resolution over Asia. The boundary condition is generated with a global-scale 4°x5° resolution simulation.

The anthropogenic emission inventories are identical to those used in Jiang et al. (2013). The global anthropogenic emission inventory is EDGAR 3.2FT2000 (Olivier et al., 2001), updated by the following regional emission inventories: the INTEX-B Asia emissions inventory for 2006 (Zhang et al., 2009b), the Cooperative Program for Monitoring and Evaluation of the Long-range Transmission of Air Pollutants in Europe (EMEP) inventory for Europe in 2000

(Vestreng et al., 2002), the US Environmental Protection Agency National Emission Inventory (NEI) for 2005 in North America, the Criteria Air Contaminants (CAC) inventory for Canada, and the Big Bend Regional Aerosol and Visibility Observational (BRAVO) Study Emissions Inventory for Mexico (Kuhns et al., 2003). Biomass burning emissions are from the inter-annual GFED3 inventory with 3-hour resolution (van der Werf et al., 2010). The biogenic emissions are from MEGAN 2.0 (Millet et al. 2008). Figure 1 shows the anthropogenic emission of NO_x and CO in Asia in June 2006. There are strong pollutant emissions in the North China Plain. The urban emission centers can also be clearly identified. The annual anthropogenic NO_x emission over Eastern China is 16.5Tg (2006) and 20.7Tg (2010), with a 5% annual growth rate.

3. Inversion Approach

3.1. 4DVAR inversion for global CO emission

In this work, we evaluate the observed interannual variability of O_3 and CO and the GEOS-Chem model simulation for the period of 2006 to 2010, where the data density of TES measurements is higher relative to subsequent years. As the first year of this five-year period, the relative contributions of O_3 precursors to free troposphere O_3 in 2006 will be studied in detail. The 2006 global CO emissions are optimized with a 4DVAR method. The inverse method minimizes the cost function $J(\mathbf{x})$ to provide an optimal estimate of the CO sources,

$$J(\mathbf{x}) = (\mathbf{F(x)} - \mathbf{y})^{\mathrm{T}} \mathbf{S}_{\Sigma}^{-1} (\mathbf{F(x)} - \mathbf{y}) + (\mathbf{x} - \mathbf{x}_{\mathbf{a}})^{\mathrm{T}} \mathbf{S}_{\mathbf{a}}^{-1} (\mathbf{x} - \mathbf{x}_{\mathbf{a}}) \quad (3)$$

where $\mathbf{x}$ is the state vector of emissions, $\mathbf{x}_{\mathbf{a}}$ is the a priori estimate, $\mathbf{y}$ is a vector of observed concentrations, and $\mathbf{F(x)}$ is the forward model, which represents the transport of the CO emissions in the GEOS-Chem model and accounts for the vertical smoothing of the MOPITT retrieval. $\mathbf{S}_{\Sigma}$ and $\mathbf{S}_{\mathbf{a}}$ are the observational and a priori error covariance matrices, respectively.

185 The first term of the cost function represents the mismatch between the simulated and observed
186 concentrations. The second term represents the departure of the estimate from the a priori.

187 The cost function in Equation 3 is minimized by reducing the gradient, $\partial J/\partial x$, using the
188 adjoint of GEOS-Chem model in a 4DVAR approach (Henze et al., 2007), which has been
189 previously used for assimilation of CO and O_3 (Kopacz et al., 2010; Singh et al. 2011; Parrington
190 et al., 2012; Jiang et al., 2014b). Similar as in Jiang et al. (2013, 2014b), we produce improved
191 initial conditions by assimilating MOPITT version 6 data, using the sequential sub-optimal
192 Kalman filter (Parrington et al. 2008), from 1 January 2006 to 1 January 2007. The optimized
193 initial conditions are archived at the beginning of each month. Consequently, the initial
194 conditions for the model simulation are independent from the inverse analyses.

195 **3.2. Regression-based inversion for China NO_x emissions**

196 The 2006 Chinese NO_x emissions are optimized with a regression-based multi-step
197 method exploiting the distinctive seasonality of different sources (Lin 2012). Neglecting
198 horizontal transport and assuming a linear relationship between the total VCD of NO_2 and VCDs
199 from individual sources, the predicted VCD (Ω_p) for a given grid can be expressed as the sum
200 of individual emission sources, multiplied by certain scaling factors:

201 $$\Omega_p = k_a\Omega_a + k_l\Omega_l + k_s\Omega_s + k_b\Omega_b \quad (4)$$

202 The subscripts "a", "l", "s", and "b" indicate anthropogenic, lightning, soil and biomass burning
203 sources of NO_x, respectively. The updated emission estimates can be obtained by reducing the
204 sum of $[(\Omega_r - \Omega_p)/\sigma]^2$ across the 12 months; here Ω_r is the retrieved VCD and σ is the
205 standard deviation. To better represent the resolution-dependent NO_x chemistry (Valin et al.
206 2011), the inversion was conducted with the highest resolution of GEOS-Chem. The seasonality-
207 based inversion method also reduced the influence of potential biases in OMI NO_2 data (Lin et al.

208 2014b), particularly in winter. The details for the inversion process were described in Lin (2012).

209 # 4. Results and Discussion

210 ## 4.1. Evaluation of the model simulation and top-down estimates of O_3 precursors

211 In this work, we are interested in the domain of East China, as shown in Figure 1,
212 because it is the largest pollutant emission contributor in East Asia and the adjacent domain
213 where outflow of Asian pollution is significant. Figure 2 shows the monthly regional mean O_3
214 and CO concentration at free troposhere (681 - 383 hPa) for June, July and August for the period
215 2006-2010, using the GEOS-Chem model driven with a priori emission inventories. The
216 modeled O_3 concentrations are generally within 10% of the TES data after accounting for the
217 approximately 7 ppb bias in the TES O_3 measurements (e.g., H. Worden et al., 2007, Verstraeten
218 et al., 2013). On the other hand, the modeled CO is biased low, which is consistent with previous
219 studies (Shindell et al. 2006, Kopacz et al. 2010, Naik et al. 2013). This low bias could be
220 associated with a positive bias in OH, as indicated by Jiang et al. (2014b). The bias in CO can be
221 reduced by integrating the coarse-resolution global and fine-resolution nested simulations in a
222 two-way coupled manner, such that results from the nested model can be used to improve the
223 global model (within the nested domain) and ultimately affect its lateral boundary conditions (via
224 the global transport of CO and other species) (Yan et al. 2014). Another possible reason for the
225 CO bias is that the TES CO data are biased towards polluted air parcels because of its relatively
226 low sensitivity whereas the model captures background values as discussed in Pechony et al.
227 (2013). Although the model is biased low, the interannual variabilities and trends of O_3 and CO
228 are well correlated between the model and TES, indicating that changes in the modeled
229 emissions, chemical production of ozone, and meterology are well described (e.g., Zhang et al.,
230 2006; Kim et al., 2013).

231 O_3-CO correlations can be used to constrain O_3 sources and transport (e.g., Zhang et al.,
232 2006). Positive correlations usually indicate that a region has experienced photochemical O_3
233 production, whereas negative correlations may result from O_3 chemical loss or influence of
234 stratospheric air. For example, Zhang et al. (2006) demonstrated that TES data can be used to
235 examine global distribution of O_3-CO correlations. Voulgarakis et al. (2011) found significant
236 positive correlations in the northern Pacific during the summer of 2005-2008. Kim et al. (2013)
237 used OMI O_3 and AIRS CO to show that the GEOS-Chem model is able to reproduce the
238 observed O_3-CO correlations and slopes in western Pacific, but failed in some tropical regions
239 due to model transport error associated with deep convection.

240 Table 1 shows the monthly regional mean O_3 and CO correlation and slope values for the
241 free troposphere (825 - 383 hPa) for June, July and August 2006-2010; the model is driven by a
242 priori emissions. The uncertainty in the O_3 and CO concentrations are due to random errors in
243 the TES O_3 and CO observations and natural variability (Zhang et al., 2006). For this reason, we
244 also show the mean value over the analysis time period. The correlation and slope values of TES
245 and GEOS-Chem are generally consistent for both domains. The positive correlation coefficients
246 imply influence of photochemical O_3 production but also transport of nearby CO emissions into
247 pollution plumes (e.g., Worden *et al.*, 2013) As in previous studies (Zhang et al. 2006;
248 Voulgarakis et al. 2011; Kim et al. 2013), there are small differences between the simulation and
249 observation. A possible reason for these discrepancies, particularly over the ocean, is the model
250 transport error because transport of "clean" air from the Pacific can have substantially different
251 chemical charateristics from Asian air.

252 The consistency between model and TES in the interannual varations, correlation
253 coefficients and slopes implies that the spatio-temporal distribution of the CO emissions and

254 oxidative chemical processes are consistent. As described in Section 3, the 2006 global CO
255 emission are constrained with MOPITT data; the 2006 Chinese NO_x emission are constrained
256 with OMI data. As shown in Figure 3, Chinese *posterior* anthropogenic NO_x emissions in June
257 2006 are increased by 14% over the *a priori* emissions, from 1.86 Tg to 2.11 Tg. Smaller
258 adjustments are obtained for winter. In June 2006, the Chinese anthropogenic CO emissions are
259 increased from 17.09 Tg to 18.93 Tg, with a mean scaling factor of 1.11. In December 2005, the
260 Chinese *posterior* anthropogenic CO emission is increased over the *prior* from 14.95 Tg to 19.78
261 Tg.. However, as indicated by Jiang et al. (2014b), a potential bias in OH fields could have a
262 significant influence on the inferred CO emission estimates. By using the OH fields from a
263 different GEOS-Chem version, they found that a posteriori CO emissions over East Asia in June
264 - August 2004 are reduced by 28% for the different OH fields. This large potential error in the
265 CO emissions do not strongly affect our conclusions because the modeled CO concentrations,
266 based on the model OH distributions and CO emissions, are consistent with the MOPITT data.

267 The monthly regional mean O_3 and CO concentrations in the period of Dec 2005 -Nov
268 2006 are shown in Figure 4. In order to remove the influence of the initial conditions, the
269 updated-simulation is obtained by running the model from 1 September 2005, with updated
270 inventories of NO_x and CO. Both model and data shows increase of O_3 concentration from
271 winter to spring, due to enhancement of photochemical production, and a substantial decrease in
272 Jun – Aug, due to the effect of East Asian monsoon (Yang et al. 2014). The CO concentration
273 peaks in March, which is consistent with Shindell et al. (2006). The boreal spring CO maximum
274 is associated with the accumulation of CO emission in winter, while CO lifetime is longer
275 (Ducan et al. 2007). The updated inventories significantly reduced the bias on the CO simulation.
276 However, these changes in the NOx and CO emissions do not significantly change free-

277 tropospheric ozone.

278 **4.2. Dependency of O_3 on anthropogenic and natural NO_x, CO and VOCs**

279 In this section, we will use the adjoint of the GEOS-Chem model (Henze et al., 2007) to
280 quantify source contributions (NO_x, CO, VOC) to free tropospheric O_3 pollution over East China
281 and the China Outflow region. The updated NO_x and CO emission inventories is intended to
282 improve the simulation. We are interested in these two domains as they have significant
283 influence on the long-range pollution transport (e.g., Zhang et al., 2009a). Similar to previous
284 studies (Zhang et al. 2009; Bowman et al. 2012; Lapina et al. 2014), the analysis is based on a
285 sensitivity calculation from an adjoint model. In this work, both transport and chemistry
286 components are run backwards and thus provide a more computationally efficient method for a
287 receptor-oriented problem than the traditional approach by perturbing emissions.

288 Figure 5 shows the contributions of anthropogenic NO_x, lightning NO_x, anthropogenic
289 CO and biogenic isoprene on free tropospheric (819 - 396 hPa) O_3 over eastern China. The value
290 can be explained as the percentage change of regional mean O_3 due to a fractional change in
291 emissions in a particular grid. For example, assuming an unchanged chemical environment, one
292 particular grid with contribution 0.02% implies mean free tropospheric O_3 over eastern China
293 will be increased by 0.02%, if the NO_x emission in this gird is increased by 100%. The result
294 shows that anthropogenic NO_x contributes significantly to the O_3 distribution in this region.
295 Although the influence of lightning NO_x is weaker, the larger geographical distribution of
296 lightning NO_x makes it an important source. The contribution of anthropogenic CO is mainly
297 from China, whereas Southeast Asia is the major contributor of biogenic isoprene with a
298 negative sensitivity. Assuming anthropogenic CO is a proxy of anthropogenic hydrocarbons and
299 biogenic isoprene is a proxy of biogenic hydrocarbons, these sensitivity calculations indicates

300 that China is a major source of anthropogenic hydrocarbons while Southeast Asia is the major
301 source of biogenic hydrocarbons. As shown in Figure 1, the North China Plain has strong NO_x
302 emission, but its effect on O_3 is not significant. On the other hand, Eastern China free-
303 tropospheric O_3 is more directly sensitive to CO emission from North China Plain. The
304 contribution of CO to ozone production (3^{rd} set of panels in Figure 5) is similar to the CO
305 emission distribution. Discrepancies exist between the spatial distribution of the sensitivity of
306 ozone to NO_x and CO. For example, the sensitivity of ozone to NO_x in the Bejing area is
307 relatively small because there is too much NO_x, thus limiting ozone production. Martin et al.
308 (2004) showed that an increase of NO_x emission over northeast China in summer will decrease
309 surface O_3 concentration, which is opposite with the positive sensitivity in this work. This
310 difference could be associated with the larger concentrations of VOC levels (e.g., Martin et al.
311 2006; Zhang et al. 2014) and because the sensitivities shown in Figure 5 depend on both surface
312 ozone production and ozone production in the free-troposphere, which is more NOx limited.
313 It should be reminded that the sensitivity of ozone to biogenic isoprene is highly
314 dependent on the isoprene chemistry scheme, as indicated by Mao et al. (2013). They
315 demonstrated that the sensitivity of surface O_3 concentration over southeast United States on
316 isoprene could change sign, from negative to positive, with two different isoprene schemes.
317 However, as shown in Figure 5 the influence of the isoprene scheme on free tropospheric O_3 is
318 small relative to that from NOx so that we do not expect that errors in the isoprene scheme to
319 significantly alter our conclusions. These results are consistent with Mao et al. (2013) as they
320 show that a change in sign in the sensitivity of ozone to isoprene only affected their surface
321 ozone concentrations by 2 ppb or less and therefore an even smaller effect on free-tropospheric
322 ozone concentrations.

323 The contributions to the free tropospheric ozone in the the China Outflow region are
324 shown in Figure 6. The O_3 distribution is more sensitive to the anthropogenic NO_x emission from
325 the coast rather than from the inland continent. The sensitivity hotspots clearly show a
326 northeastward movement as the season progresses, from Southeast China (June) to Korea and
327 Japan (August), reflecting the influence of the East Asia monsoon.
328 To understand the seasonal variation of O_3 production efficiency, we calculated the
329 global scale sensitivities of anthropogenic and lightning NO_x during December 2005 – November
330 2006 with 4°x5° resolution. The values of sensitivities, as shown in Figure 7, are significantly
331 larger than those in Figure 5 and Figure 6, due to the change of grid size and smaller effect from
332 initial condition. The sensitivity of O_3 to anthropogenic $NO_{x,,}$ has a marked seasonal variation,
333 increasing from the Northern Hemisphere winter to the summer. Kondo et al. (2008) found the
334 slope of East Asia O_3 formation to NO_x is proportional to HO_2 and thus increases from winter to
335 spring. Increased solar radiation is another reason for the high O_3 production rate in the summer.
336 Figure 7 also highlights the effect of anthropogenic NO_x from southwest China, showing a
337 significant effect on free troposphere O_3 over eastern China, particularly in September-
338 November. Similar to anthropogenic NO_x, the contribution of lightning NO_x is maximum in the
339 Northern Hemisphere summer, partly associated with the East Asia monsoon. The sensitivities of
340 O_3 over eastern China and the China Outflow region have similar distributions, although the
341 China Outflow O_3 is more sensitive to coastal emissions.
342 Table 2 shows the regional total contributions of anthropogenic and lightning NO_x,
343 calculated by summing the sensitivities shown in Figure 7. Assuming an unchanged chemical
344 environment, it can be explained as the percentage change of regional mean O_3 due to 100%
345 change in NO_x emission. For example, a 100% increase of Chinese anthropogenic NO_x emission

346 in June-August 2006 will result in 10.2% increase of tropospheric mean O_3 over eastern China.
347 Of course, the result of an actual 100% change of NO_x will be different to quantify because of
348 non-linear chemistry. Furthermore, this sensitivity depends on the modeled transport and the
349 robustness of the chemical production of ozone. For example, if the production of ozone is too
350 "fast" then the sensitivity of free-tropospheric ozone to surface emissions is too small as too
351 much ozone is produced in the boundary layer (where loss-mechanisms dominate) versus the
352 free-troposphere. To evaluate the sensitivities further, we enhanced Chinese anthropogenic NO_x
353 emission by 10% uniformly as a perturbation. Using the initial conditions provided from
354 standard simulation, the 3-month perturbation simulations are started on 1 December 2005, 1
355 March 2006, 1 June 2006 and 1 September 2006, individually. The relative difference of regional
356 mean O_3, between the perturbation and standard simulations, is then multiplied by 10. As shown
357 in Table 2, the results of two methods are highly consistent, which demonstrates our sensitivity
358 analysis works well. Similar as Wild et al. (2012), the consistency also confirms that 10% NO_x
359 perturbation gives a linear O_3 responses over East Asia. Considering the high computation
360 efficiency, adjoint sensitivity analysis is thus a good alternative to the traditional perturbation
361 method.

362 As shown in Table 2, the effect of increased Chinese anthropogenic NO_x on free
363 tropospheric O_3 is limited. Assuming an unchanged chemical environment, a 100% increase of
364 Chinese anthropogenic NO_x, during a 3-month period, will only result in 2.4% increase of free
365 tropospheric O_3 in the winter and 10.2% in the summer, associated with the chemical
366 environment of China, which is is more inclined to be VOC limited. Because of the long O_3
367 lifetime in the free troposphere, O_3 from initial conditions have a substantial influence on the
368 distribution of ozone. A 15-month continous perturbation simulation, started on 1 September

2005, will enhance the effect of Chinese anthropogenic NO_x to 3.0% in winter and 10.5% in summer.

Because of the rapid growth of pollutant emission, transpacific transport of Asian pollutant to North America has attractted significant attention (Zhang et al. 2008, 2009; Walker et al. 2010; Bertram et al. 2013; Lin et al. 2008, 2014a). The major transport mechanisms includes northeastward export of Asian pollution to about 50°N, and then cross the Pacific in midlatitude westerly winds (Liang et al. 2004, 2005). Over eastern China, the effect of anthrogogenic NO_x emission from the Rest of Asia (ROA) on free tropospheric O_3 is about 50% of Chinese local emission in winter and spring, whereas Chinese local emission dominates in the summer and fall. Our results show that the influence of ROA on O_3 pollution export is significant because the influence of ROA is comparable with Chinese emisisons in winter and about 50% of Chinese emissions in other seasons for the outflow region. The contribution of lightning NO_x over China is generally small relative to anthropogenic emisisons except during the summer (Table 2). The effect of ROA lightning NO_x is similar as the Chinese contribution but slightly larger.

5. Summary

We quantified Asian O_3 and the contributions of its precursors, during the period December 2005 – November 2006, using the GEOS-Chem model and O_3 precursor observations of NO_2 from OMI and CO from MOPITT. The 2006 global CO emissions are constrained with a 4DVAR method, using MOPITT CO (version 6) measurements. In June 2006, the inversion increases the China anthropogenic CO emission by 11%. The 2006 China NO_x emission is constrained with a regression-based multi-step approach, using OMI data. In June 2006, the anthropogenic NO_x emission in China is increased by 14%.

The model simulation is evaluated with TES O_3 and CO observations. The modeled concentrations are underestimated for both O_3 and CO, but reproduces the O_3(CO) interannual varation. As with previous studies (Zhang et al. 2006; Voulgarakis et al. 2011; Kim et al. 2013), the modeled O_3-CO correlation and slope are consistent with the data. The updated inventories significantly reduces the bias relative to TES CO measurements. But the improvement on the O_3 simulation is not large (~1-2%). The good agreement between model O_3 and CO and its correlations with observations from TES demonstrate the reliability of the model simulation, the chemical scheme and the updated CO inventories.

We quantified source contributions (NO_x, CO, VOC) to free tropospheric O_3 pollution over East China and the China Outflow region with a sensitivity calculation approach. Our results show anthropogenic emissions from China is the major contributor on free tropospheric O_3 over Eastern Asia and corresponding outflow region. The anthropogenic emissions from the Rest-of-Asia (ROA) has an important influence on free tropospheric O_3 over this region. The observed seasonal variation in O_3 is due to the seasonal change in the O_3 production efficiency, related with HO_2 and solar radiation. The contributions of lightning NO_x to free-tropospheric O_3 from China and ROA is small, except in June-August due to the effect of the East Asia monsoon. Finally, our result shows that China is the major contributor of anthropogenic VOCs, whereas the influence of biogenic VOCs is mainly from Southeast Asia.

6. Acknowledgments.

Part of this research was carried out at the Jet Propulsion Laboratory, California Institute of Technology, under a contract with the National Aeronautics and Space Administration. This Research was supported by the NASA ROSES Aura Science Team NNH10ZDA001N-AURA. Daven K. Henze was funded by NASA ACMAP NNX13AK86G. Willem W. Verstraeten was

415 funded by the Netherlands Organization for Scientific Research, NWO Vidi grant 864.09.001.

416

417 7. References

418 Beer, R., Glavich, T. A., and Rider, D. M.: Tropospheric emission spectrometer for the Earth
419 Observing System's Aura satellite, Appl. Optics, 40, 2356–2367, 2001.

420 Bertram, T. H., Perring, A. E., Wooldridge, P. J., Dibb, J., Avery, M. A., and Cohen, R. C.: On
421 the export of reactive nitrogen from Asia: NO_x partitioning and effects on ozone, Atmos. Chem.
422 Phys., 13, 4617–4630, doi:10.5194/acp-13-4617-2013, 2013.

423 Boersma, K. F., Eskes, H. J., Dirksen, R. J., van der A, R. J., Veefkind, J. P., Stammes, P.,
424 Huijnen, V., Kleipool, Q. L., Sneep, M., Claas, J., Leitão, J., Richter, A., Zhou, Y., and
425 Brunner, D.: An improved tropospheric NO_2 column retrieval algorithm for the Ozone
426 Monitoring Instrument, Atmos. Meas. Tech., 4, 1905–1928, doi:10.5194/amt-4-1905-2011,
427 2011.

428 Bowman, K. and Henze, D. K.: Attribution of direct ozone radiative forcing to spatially resolved
429 emissions, Geophys. Res. Lett., 39, L22704, doi:10.1029/2012GL053274, 2012.

430 Brown-Steiner, B. and Hess, P.: Asian influence on surface ozone in the United States: a
431 comparison of chemistry, seasonality, and transport mechanisms, J. Geophys. Res., 116,
432 D17309, 2011.

433 Chen, D., Wang, Y., McElroy, M. B., He, K., Yantosca, R. M., and Le Sager, P.: Regional CO
434 pollution and export in China simulated by the high-resolution nested-grid GEOS-Chem model,
435 Atmos. Chem. Phys., 9, 3825–3839, doi:10.5194/acp-9-3825-2009, 2009.

436 Deeter, M. N., Martínez-Alonso, S., Edwards, D. P., Emmons, L. K., Gille, J. C., Worden, H. M.,
437 Pittman, J. V., Daube, B. C., and Wofsy, S. C.: Validation of MOPITT Version 5 thermal-

infrared, near-infrared, and multispectral carbon monoxide profile retrievals for 2000–2011, J. Geophys. Res.-Atmos., 118, 6710–6725, 2013.

Duncan, B. N., Logan, J. A. Bey, I., Megretskaia, I. A., Yantosca, R. M., Novelli, P. C., Jones, N. B., and Rinsland, C. P.: Global budget of CO, 1988–1997: Source estimates and validation with a global model, J. Geophys. Res., 112, D22301, doi:10.1029/2007JD008459, 2007.

Fortems-Cheiney, A., Chevallier, F., Pison, I., Bousquet, P., Szopa, S., Deeter, M. N., and Clerbaux, C.: Ten years of CO emissions as seen from Measurements of Pollution in the Troposphere (MOPITT), J. Geophys. Res., 116, D05304, doi:10.1029/2010JD014416, 2011.

Fu, T.-M., Jacob, D. J., Palmer, P. I., Chance, K., Wang, Y. X., Barletta, B., Blake, D. R., Stanton, J. C., and Pilling, M. J.: Space-based formaldehyde measurements as constraints on volatile organic compound emissions in east and south Asia and implications for ozone, J. Geophys. Res., 112, D06312, doi:10.1029/2006JD007853, 2007.

Gonzi, S., Feng, L., and Palmer, P. I.: Seasonal cycle of emissions of CO inferred from MOPITT profiles of CO: sensitivity to pyroconvection and profile retrieval assumptions, Geophys. Res. Lett., 38, L08813, doi:10.1029/2011GL046789, 2011.

Henze, D. K., Hakami, A., and Seinfeld, J. H.: Development of the adjoint of GEOS-Chem, Atmos. Chem. Phys., 7, 2413–2433, doi:10.5194/acp-7-2413-2007, 2007.

Jiang, Z., Jones, D. B. A., Worden, H. M., Deeter, M. N., Henze, D. K., Worden, J., Bowman, K. W., Brenninkmeijer, C. A. M., and Schuck, T. J.: Impact of model errors in convective transport on CO source estimates inferred from MOPITT CO retrievals, J. Geophys. Res.-Atmos., 118, 2073–2083, 2013.

Jiang, Z., Jones, D. B. A., Henze, D., Worden, H., Wang, Y. X.: Regional data assimilation of multi-spectral MOPITT observations of CO over North America, 2014, in preparation.

461 Jiang, Z., Jones, D. B. A., Henze, D., Worden, H: Sensitivity of inferred regional CO source
462 estimates to the vertical structure in CO as observed by MOPITT, Atmos. Chem. Phys.
463 Discuss., 14, 22939-22984, doi:10.5194/acpd-14-22939-2014, 2014b.
464 Jones, D. B. A., Bowman, K. W., Logan, J. A., Heald, C. L., Liu, J., Luo, M., Worden, J., and
465 Drummond, J.: The zonal structure of tropical O_3 and CO as observed by the Tropospheric
466 Emission Spectrometer in November 2004 – Part 1: Inverse modeling of CO emissions, Atmos.
467 Chem. Phys., 9, 3547–3562, doi:10.5194/acp-9-3547-2009, 2009.
468 Kim, P. S., Jacob, D. J., Liu, X., Warner, J. X., Yang, K., Chance, K., Thouret, V., and Nedelec,
469 P.: Global ozone–CO correlations from OMI and AIRS: constraints on tropospheric ozone
470 sources, Atmos. Chem. Phys., 13, 9321–9335, doi:10.5194/acp-13-9321-2013, 2013.
471 Kondo, J., Hudman, R. C., Nakamura, K., Koike, M., Chen, G., Miyazaki, Y., Takegawa, N.,
472 Blake, D. R., Simpson, I. J., Ko, M., Kita, K., and Shirai, T.: Mechanisms that influence the
473 formation of high-ozone regions in the boundary layer downwind of the Asian continent in
474 winter and spring, J. Geophys. Res., 113, D15304, doi:10.1029/2007JD008978, 2008.
475 Kopacz, M., Jacob, D. J., Fisher, J. A., Logan, J. A., Zhang, L., Megretskaia, I. A., Yantosca, R.
476 M., Singh, K., Henze, D. K., Burrows, J. P., Buchwitz, M., Khlystova, I., McMillan, W. W.,
477 Gille, J. C., Edwards, D. P., Eldering, A., Thouret, V., and Nedelec, P.: Global estimates of CO
478 sources with high resolution by adjoint inversion of multiple satellite datasets (MOPITT, AIRS,
479 SCIAMACHY, TES), Atmos. Chem. Phys., 10, 855-876, doi:10.5194/acp-10-855-2010, 2010.
480 Kuhns, H., Green, M., and Etyemezian, V.: Big Bend Regional Aerosol and Visibility
481 Observational (BRAVO) Study Emissions Inventory, Report prepared for BRAVO Steering
482 Committee, Desert Research Institute, Las Vegas, Nevada, 2003.
483 Lamsal, L. N., Martin, R. V., Padmanabhan, A., van Donkelaar, A., Zhang, Q., Sioris, C. E.,

484 Chance, K., Kurosu, T. P., and Newchurch, M. J.: Application of satellite observations for
485 timely updates to global anthropogenic NOx emission inventories, Geophys. Res. Lett., 38,
486 L05810, doi:10.1029/2010GL046476, 2011.
487 Lapina, K., Henze, D. K., Milford, J. B., Huang, M., Lin, M., Fiore, A. M., Carmichael, G.,
488 Pfister, G. G., and Bowman, K.: Assessment of source contributions to seasonal vegetative
489 exposure to ozone in the U.S., J. Geophys. Res.-Atmos., 119, 324–340, 2014.
490 Levelt, P. F., van den Oord, G. H. J., Dobber, M. R., Malkki, A., Visser, H., de Vries, J.,
491 Stammes, P., Lundell, J. O. V., and Saari, H.: The Ozone Monitoring Instrument, IEEE T.
492 Geosci. Remote, 44, 1093–1101, 2006.
493 Liang, Q., Jaegle, L., Jaffe, D. A., Weiss-Penzias, P., Heckman, A., and Snow, J. A.: Long-
494 range transport of Asian pollution to the northeast Pacific: seasonal variations and transport
495 pathways of carbon monoxide, J. Geophys. Res., 109, D23S07, doi:10.1029/2003JD004402,
496 2004.
497 Liang, Q., Jaegle, L., and Wallace, J. M.: Meteorological indices for Asian outflow and
498 transpacific transport on daily to interannual timescales, J. Geophys. Res., 110, D18308,
499 doi:10.1029/2005JD005788, 2005.
500 Lin, J.-T., Wuebbles, D. J., and Liang, X. Z.: Effects of intercontinental transport on surface
501 ozone over the United States: present and future assessment with a global model, Geophys.
502 Res. Lett., 35, L02805, doi:10.1029/2007GL031415, 2008.
503 Lin, J.-T. and McElroy, M. B.: Detection from space of a reduction in anthropogenic emissions
504 of nitrogen oxides during the Chinese economic downturn, Atmos. Chem. Phys., 11, 8171–
505 8188, doi:10.5194/acp-11-8171-2011, 2011.
506 Lin, J.-T.: Satellite constraint for emissions of nitrogen oxides from anthropogenic, lightning and

soil sources over East China on a high-resolution grid, Atmos. Chem. Phys., 12, 2881–2898, doi:10.5194/acp-12-2881-2012, 2012.

Lin, J.-T., Liu, Z., Zhang, Q., Liu, H., Mao, J., and Zhuang, G.: Modeling uncertainties for tropospheric nitrogen dioxide columns affecting satellite-based inverse modeling of nitrogen oxides emissions, Atmos. Chem. Phys., 12, 12255–12275, doi:10.5194/acp-12-12255-2012, 2012b.

Lin, J.-T., Pan, D., Davis, S. J., Zhang, Q., He, K., Wang, C., Streets, D. G., Wuebbles, D. J., and Guan, D.: China's international trade and air pollution in the United States, P. Natl. Acad. Sci. USA, doi:10.1073/pnas.1312860111, 2014a.

Lin, J.-T., Martin, R. V., Boersma, K. F., Sneep, M., Stammes, P., Spurr, R., Wang, P., Van Roozendael, M., Clémer, K., and Irie, H.: Retrieving tropospheric nitrogen dioxide from the Ozone Monitoring Instrument: effects of aerosols, surface reflectance anisotropy, and vertical profile of nitrogen dioxide, Atmos. Chem. Phys., 14, 1441–1461, doi:10.5194/acp- 14-1441-2014, 2014b.

Liu, J. and Mauzerall, D. L.: Estimating the average time for inter-continental transport of air pollutants, Geophys. Res. Lett., 32, L11814, doi:10.1029/2005GL022619, 2005.

Luo, M., Rinsland, C., Fisher, B., Sachse, G., Diskin, G., Logan, J., Worden, H., Kulawik, S., Osterman, G., Eldering, A., Herman, R., and Shephard, M.: TES carbon monoxide validation with DACOM aircraft measurements during INTEX-B 2006, J. Geophys. Res., 112, D24S48, doi:10.1029/2007JD008803, 2007.

Mao, J., Paulot, F., Jacob, D. J., Cohen, R. C., Crounse, J. D., Wennberg, P. O., Keller, C. A., Hudman, R. C., Barkley, M. P., and Horowitz, L. W.: Ozone and organic nitrates over the eastern United States: sensitivity to isoprene chemistry, J. Geophys. Res.-Atmos., 118, 11256–

11268, doi:10.1002/jgrd.50817, 2013.

Mao, Y. H., Li, Q. B., Henze, D. K., Jiang, Z., Jones, D. B. A., Kopacz, M., He, C., Qi, L., Gao, M., Hao, W.-M., and Liou, K.-N.: Variational estimates of black carbon emissions in the western United States, Atmos. Chem. Phys. Discuss., 14, 21865-21916, doi:10.5194/acpd-14-21865-2014, 2014.

Martin, R. V., Fiore, A. M., and Donkelaar, A. Van: Space-based diagnosis of surface ozone sensitivity to anthropogenic emissions, Geophys. Res. Lett., 31, L06120, doi:10.1029/2004GL019416, 2004.

Mijling, B., van der A, R. J., and Zhang, Q.: Regional nitrogen oxides emission trends in East Asia observed from space, Atmos. Chem. Phys., 13, 12003–12012, doi:10.5194/acp-13- 12003-2013, 2013.

Millet, D. B., Jacob, D. J., Boersma, K. F., Fu, T. M., Kurosu, T. P., Chance, K., Heald, C. L., and Guenther, A.: Spatial distribution of isoprene emissions from North America derived from formaldehyde column measurements by the OMI satellite sensor, J. Geophys. Res., 113, D02307, doi:10.1029/2007JD008950, 2008.

Naik, V., Voulgarakis, A., Fiore, A. M., Horowitz, L. W., Lamarque, J.-F., Lin, M., Prather, M. J., Young, P. J., Bergmann, D., Cameron-Smith, P. J., Cionni, I., Collins, W. J., Dalsøren, S. B., Doherty, R., Eyring, V., Faluvegi, G., Folberth, G. A., Josse, B., Lee, Y. H., MacKenzie, I. A., Nagashima, T., van Noije, T. P. C., Plummer, D. A., Righi, M., Rumbold, S. T., Skeie, R., Shindell, D. T., Stevenson, D. S., Strode, S., Sudo, K., Szopa, S., and Zeng, G.: Preindustrial to present-day changes in tropospheric hydroxyl radical and methane lifetime from the Atmospheric Chemistry and Climate Model Intercomparison Project (ACCMIP), Atmos. Chem. Phys., 13, 5277-5298, doi:10.5194/acp-13- 5277-2013, 2013.

553 Olivier, J. G. J. and Berdowski, J. J. M.: Global emissions sources and sinks, in: The Climate
554 System, edited by: Berdowski, J., Guicherit, R., and Heij, B. J., 33–78, A. A. Balkema
555 Publishers/Swets & Zeitlinger Publishers, Lisse, the Netherlands, 2001.
556 Parrington, M., Jones, D. B. A., Bowman, K. W., Horowitz, L. W., Thompson, A. M., Tarasick,
557 D. W., and Witte, J. C.: Estimating the summertime tropospheric ozone distribution over North
558 America through assimilation of observations from the Tropospheric Emission Spectrometer, J.
559 Geophys. Res., 113, D18307, doi:10.1029/2007JD009341, 2008.
560 Parrington, M., Palmer, P. I., Henze, D. K., Tarasick, D. W., Hyer, E. J., Owen, R. C., Helmig,
561 D., Clerbaux, C., Bowman, K. W., Deeter, M. N., Barratt, E. M., Coheur, P.-F., Hurtmans, D.,
562 Jiang, Z., George, M., and Worden, J. R.: The influence of boreal biomass burning emissions
563 on the distribution of tropospheric ozone over North America and the North Atlantic during
564 2010, Atmos. Chem. Phys., 12, 2077–2098, doi:10.5194/acp-12-2077-2012, 2012.
565 Pechony, O., Shindell, D. T., and Faluvegi, G.: Direct top-down estimates of biomass burning
566 CO emissions using TES and MOPITT versus bottom-up GFED inventory, J. Geophys. Res.-
567 Atmos., 118, 8054–8066, doi:10.1002/jgrd.50624, 2013.
568 Shim, C., Wang, Y., Choi, Y., Palmer, P. I., Abbot, D. S., and Chance, K.: Constraining global
569 isoprene emissions with Global Ozone Monitoring Experiment (GOME) formaldehyde column
570 measurements, J. Geophys. Res., 110, D24301, doi:10.1029/2004JD005629, 2005.
571 Shindell, D. T., Faluvegi, G., Stevenson, D. S., Krol, M. C., Emmons, L. K., Lamarque, J. F.,
572 Pétron, G., Dentener, F. J., Ellingsen, K., Schultz, M. G., Wild, O., Amann, M., Atherton, C. S.,
573 Bergmann, D. J., Bey, I., Butler, T., Cofala, J., Collins, W. J., Derwent, R. G., Doherty, R. M.,
574 Drevet, J., Eskes, H. J., Fiore, A. M., Gauss, M., Hauglustaine, D. A., Horowitz, L. W., Isaksen,
575 I. S. A., Lawrence, M. G., Montanaro, V., Müller, J. F., Pitari, G., Prather, M. J., Pyle, J. A.,

576 Rast, S., Rodriguez, J. M., Sanderson, M. G., Savage, N. H., Strahan, S. E., Sudo, K., Szopa, S.,
577 Unger, N., van Noije, T. P. C., and Zeng, G.: Multimodel simulations of carbon monoxide:
578 Comparison with observations and projected near-future changes, J. Geophys. Res., 111,
579 D19306, 10.1029/2006JD007100 2006.
580 Singh, K., Jardak, M., Sandu, A., Bowman, K., Lee, M., and Jones, D.: Construction of non-
581 diagonal background error covariance matrices for global chemical data assimilation, Geosci.
582 Model Dev., 4, 299–316, doi:10.5194/gmd-4-299-2011, 2011.
583 Valin, L. C., Russell, A. R., Hudman, R. C., and Cohen, R. C.: Effects of model resolution on the
584 interpretation of satellite NO_2 observations, Atmos. Chem. Phys., 11, 11647–11655,
585 doi:10.5194/acp-11-11647-2011, 2011.
586 van der Werf, G. R., Randerson, J. T., Giglio, L., Collatz, G. J., Mu, M., Kasibhatla, P. S.,
587 Morton, D. C., DeFries, R. S., Jin, Y., and van Leeuwen, T. T.: Global fire emissions and the
588 contribution of deforestation, savanna, forest, agricultural, and peat fires (1997–2009), Atmos.
589 Chem. Phys., 10, 11707–11735, doi:10.5194/acp-10-11707-2010, 2010.
590 Verstraeten, W. W., Boersma, K. F., Zörner, J., Allaart, M. A. F., Bowman, K. W., and Worden,
591 J. R.: Validation of six years of TES tropospheric ozone retrievals with ozonesonde
592 measurements: implications for spatial patterns and temporal stability in the bias, Atmos. Meas.
593 Tech., 6, 1413–1423, doi:10.5194/amt-6-1413-2013, 2013.
594 Vestreng, V. and Klein, H.: Emission data reported to UNECE/EMEP, Quality assurance and
595 trend analysis and Presentation of WebDab, Norwegian Meteorological Institute, Oslo,
596 Norway, MSC-W Status Report, 2002.
597 Voulgarakis, A., Telford, P. J., Aghedo, A. M., Braesicke, P., Faluvegi, G., Abraham, N. L.,
598 Bowman, K. W., Pyle, J. A., and Shindell, D. T.: Global multi-year O_3–CO correlation patterns

599 from models and TES satellite observations, Atmos. Chem. Phys., 11, 5819–5838,
600 doi:10.5194/acp-11-5819-2011, 2011.
601 Walker, T. W., Martin, R. V., van Donkelaar, A., Leaitch, W. R., MacDonald, A. M., Anlauf, K.
602 G., Cohen, R. C., Bertram, T. H., Huey, L. G., Avery, M. A., Weinheimer, A. J., Flocke, F. M.,
603 Tarasick, D. W., Thompson, A. M., Streets, D. G., and Liu, X.: Trans-Pacific transport of
604 reactive nitrogen and ozone to Canada during spring, Atmos. Chem. Phys., 10, 8353–8372,
605 doi:10.5194/acp-10-8353-2010, 2010.
606 Wang, Y. X., McElroy, M. B., Jacob, D. J., and Yantosca, R. M.: A nested grid formulation for
607 chemical transport over Asia: applications to CO, J. Geophys. Res., 109, D22307,
608 doi:10.1029/2004JD005237, 2004.
609 Wang, Y., Konopka, P., Liu, Y., Chen, H., Müller, R., Plöger, F., Riese, M., Cai, Z., and Lü, D.:
610 Tropospheric ozone trend over Beijing from 2002–2010: ozonesonde measurements and
611 modeling analysis, Atmos. Chem. Phys., 12, 8389–8399, doi:10.5194/acp-12-8389-2012, 2012.
612 Wild, O., Fiore, A. M., Shindell, D. T., Doherty, R. M., Collins, W. J., Dentener, F. J., Schultz,
613 M. G., Gong, S., MacKenzie, I. A., Zeng, G., Hess, P., Duncan, B. N., Bergmann, D. J., Szopa,
614 S., Jonson, J. E., Keating, T. J., and Zuber, A.: Modelling future changes in surface ozone: a
615 parameterized approach, Atmos. Chem. Phys., 12, 2037–2054, doi:10.5194/acp-12-2037-2012,
616 2012.
617 Worden, H. M., Logan, J. A., Worden, J. R., Beer, R., Bowman, K., Clough, S. A., Eldering, A.,
618 Fisher, B. M., Gunson, M. R., Herman, R. L., Kulawik, S. S., Lampel, M. C., Luo, M.,
619 Megretskaia, I. A., Osterman, G. B., and Shephard, M. W.: Comparisons of Tropospheric
620 Emission Spectrometer (TES) ozone profiles to ozonesondes: methods and initial results, J.
621 Geophys. Res., 112, D03309, doi:10.1029/2006JD007258, 2007.

622 Worden, H. M., Deeter, M. N., Edwards, D. P., Gille, J. C., Drummond, J. R., and Nédélec, P.:
623 Observations of near surface carbon monoxide from space using MOPITT multispectral
624 retrievals, J. Geophys. Res., 115, D18314, doi:10.1029/2010JD014242, 2010.
625 Worden, J., Wecht, K., Frankenberg, C., Alvarado, M., Bowman, K., Kort, E., Kulawik, S., Lee,
626 M., Payne, V. and Worden, H.: CH_4 and CO distributions over tropical fires during October
627 2006 as observed by the Aura TES satellite instrument and modeled by GEOS-Chem,
628 Atmospheric Chemistry and Physics, 13(7), 3679–3692, doi:10.5194/acp-13-3679-2013, 2013.
629 Yan, Y.-Y., Lin, J.-T., Kuang, Y., Yang, D.-W., and Zhang, L.: Tropospheric carbon monoxide
630 over the Pacific during HIPPO: two-way coupled simulation of GEOS-Chem and its multiple
631 nested models, Atmos. Chem. Phys., submitted, 2014.
632 Yang, Y., Liao, H., and Li, J.: Impacts of the East Asian summer monsoon on interannual
633 variations of summertime surface-layer ozone concentrations over China, Atmos. Chem. Phys.,
634 14, 6867-6879, doi:10.5194/acp-14-6867-2014, 2014.
635 Zhang, L., Jacob, D. J., Bowman, K. W., Logan, J. A., Turquety, S., Hudman, R. C., Li, Q.- B.,
636 Beer, R., Worden, H. M., Worden, J. R., Rinsland, C. P., Kulawik, S. S., Lampel, M. C.,
637 Shephard, M. W., Fisher, B. M., Eldering, A., and Avery, M. A.: Ozone-CO correlations
638 determined by the TES satellite instrument in continental outflow regions, Geophys. Res. Lett.,
639 33, L18804, doi:10.1029/2006GL026399, 2006.
640 Zhang, L., Jacob, D. J., Boersma, K. F., Jaffe, D. A., Olson, J. R., Bowman, K. W., Worden, J.
641 R., Thompson, A. M., Avery, M. A., Cohen, R. C., Dibb, J. E., Flock, F. M., Fuelberg, H. E.,
642 Huey, L. G., McMillan, W. W., Singh, H. B., and Weinheimer, A. J.: Transpacific transport of
643 ozone pollution and the effect of recent Asian emission increases on air quality in North
644 America: an integrated analysis using satellite, aircraft, ozonesonde, and surface observations,

Atmos. Chem. Phys., 8, 6117–6136, doi:10.5194/acp-8-6117-2008, 2008.

Zhang, L., Jacob, D. J., Kopacz, M., Henze, D. K., Singh, K., and Jaffe, D. A.: Intercontinental source attribution of ozone pollution at western U.S. sites using an adjoint method, Geophys. Res. Lett., 36, L11810, doi:10.1029/2009GL037950, 2009a.

Zhang, Q., Streets, D. G., Carmichael, G. R., He, K. B., Huo, H., Kannari, A., Klimont, Z., Park, I. S., Reddy, S., Fu, J. S., Chen, D., Duan, L., Lei, Y., Wang, L. T., and Yao, Z. L.: Asian emissions in 2006 for the NASA INTEX-B mission, Atmos. Chem. Phys., 9, 5131–5153, doi:10.5194/acp-9-5131-2009, 2009b.

Zhang, Q., Yuan, B., Shao, M., Wang, X., Lu, S., Lu, K., Wang, M., Chen, L., Chang, C.-C., and Liu, S. C.: Variations of ground-level O_3 and its precursors in Beijing in summertime between 2005 and 2011, Atmos. Chem. Phys., 14, 6089-6101, doi:10.5194/acp-14-6089-2014, 2014.

Tables and Figures

Table 1. Monthly regional mean O_3 and CO correlation and slope for the free troposphere (825 - 383 hPa) for June, July and August 2006-2010 for both TES and model (in the parentheses). The model values are sampled at TES measurement time and location and smoothed with the TES averaging kernels. The calculation of slope and correlation is based on individual measurements within a month. The numbers of measurements used to compute the correlations are shown in the supplemental. The right column is the mean value of 15 months.

Table 2. Regional total contributions of anthropogenic and lightning NO_x on free tropospheric (819 - 396 hPa) O_3 over eastern China and the China Outflow region. The value can be explained as the percentage change of regional mean O_3 (Eastern China, China Outflow) due to 100% increase of NO_x in a particular region (China and ROA). The regions of China and ROA (Rest of Asia) are defined in Figure 3. The perturbation values (Pt) are the relative difference between standard and perturbation simulations.

Figure 1. Anthropogenic emission of (a) NO_x and (b) CO in June 2006 as used in GEOS-Chem. The unit is molec/cm^2/s. The black box defines the domains studied in this work. The "East

China" domain includes the grids of Chinese mainland within the black box. The "China Outflow region" are grids within the black box, excluding the Chinese mainland.

Figure 2. Monthly regional mean O_3 and CO concentration at free troposphere (681 - 383 hPa) in June, July and August 2006-2010. Red line is GEOS-Chem model simulation with a priori emission inventories and black line is TES measurements. The model results are smoothed wth the TES averaging kernels. The TES ozone data are biased high by 7 ppbv.

Figure 3. (a) Scaling factors of anthropogenic NO_x for June 2006. (b) Scaling factor of total CO emission (combustion + oxidation from biogenic VOCs) for June 2006.

Figure 4. Monthly regional mean O_3 and CO concentration at free troposphere (681 - 383 hPa) in the period of Dec 2005 – Nov 2006. Red line is GEOS-Chem model simulation with a priori emission inventories. Blue line is model simulation with updated NO_x and CO emission inventories. Black line is TES measurements. The model results are smoothed wth the TES averaging kernels. The positive bias in the TES O_3 data is larger in summer and smaller in winter.

Figure 5. Contributions of anthropogenic NO_x, lightning NO_x, anthropogenic CO, biogenic isoprene on free tropospheric (819 - 396 hPa) O_3 over eastern China derived from the adjoint of GEOS-Chem in June, July and August 2006. The contributions can be explained as the percentage change of regional mean ozone due to a fractional change in the emissions in a particular grid assuming unchanged chemical environment. The numbers are the total of absolute value of pre-cursor contributions for the whole domain shown in the figures.

Figure 6. Contributions of anthropogenic NOx, lightning NOx, anthropogenic CO, biogenic isoprene on free tropospheric (819 - 396 hPa) O_3 over China Outflow region derived from the adjoint of GEOS-Chem in June, July and August 2006.

Figure 7. Contributions of anthropogenic NO_x and lightning NO_x on free tropospheric (819 - 396 hPa) O_3 over eastern China and China outflow region in December 2005 – November 2006.

Region	Type	Month	2006	2007	2008	2009	2010	MEAN
Eastern China	dO3/dCO	Jun	0.36 (0.25)	0.17 (-0.06)	0.19 (0.14)	0.14 (0.02)	0.18 (0.29)	0.22 (0.25)
		Jul	0.08 (0.38)	0.29 (0.36)	0.23 (0.34)	0.15 (0.44)	0.38 (0.19)	
		Aug	0.20 (0.27)	0.22 (0.26)	0.32 (0.20)	0.15 (0.18)	0.29 (0.47)	
	R	Jun	0.66 (0.39)	0.47 (-0.11)	0.45 (0.30)	0.51 (0.10)	0.70 (0.52)	0.50 (0.37)
		Jul	0.23 (0.61)	0.66 (0.57)	0.49 (0.38)	0.50 (0.57)	0.53 (0.24)	
		Aug	0.33 (0.38)	0.52 (0.43)	0.54 (0.28)	0.39 (0.22)	0.56 (0.64)	
China Outflow	dO3/dCO	Jun	0.32 (0.60)	0.49 (0.43)	0.52 (0.62)	0.59 (0.66)	0.64 (0.76)	0.55 (0.70)
		Jul	0.56 (0.59)	0.50 (0.48)	0.65 (0.83)	0.63 (1.05)	0.75 (1.13)	
		Aug	0.55 (0.85)	0.32 (0.49)	0.51 (0.61)	0.53 (0.51)	0.67 (0.89)	
	R	Jun	0.69 (0.57)	0.71 (0.41)	0.76 (0.62)	0.68 (0.35)	0.73 (0.55)	0.67 (0.57)
		Jul	0.73 (0.57)	0.66 (0.47)	0.66 (0.69)	0.59 (0.70)	0.73 (0.78)	
		Aug	0.68 (0.71)	0.55 (0.46)	0.63 (0.60)	0.58 (0.39)	0.74 (0.75)	

Table 1. Monthly regional mean O_3 and CO correlation and slope for the free troposphere (825 - 383 hPa) for June, July and August 2006-2010 for both TES and model (in the parentheses). The model values are sampled at TES measurement time and location and smoothed with the TES averaging kernels. The calculation of slope and correlation is based on individual measurements within a month. The numbers of measurements used to compute the correlations are shown in the supplemental. The right column is the mean value of 15 months.

Type		Eastern China				China Outflow			
		DJF	MAM	JJA	SON	DJF	MAM	JJA	SON
NOx Anthro	China	2.4%	5.2%	10.2%	7.0%	2.6%	5.5%	8.6%	5.8%
	China (Pt)	2.6%	5.3%	10.2%	6.8%	2.9%	5.8%	8.5%	5.7%
	ROA	1.7%	2.0%	2.2%	2.0%	2.2%	2.4%	3.4%	2.9%
NOx lightning	China	0.2%	1.6%	6.1%	1.4%	0.3%	2.3%	6.3%	1.7%
	ROA	0.8%	2.2%	2.6%	1.9%	1.2%	3.1%	3.9%	2.8%

Table 2. Regional total contributions of anthropogenic and lightning NO_x on free tropospheric (819 - 396 hPa) O_3 over eastern China and the China Outflow region. The value can be explained as the percentage change of regional mean O_3 (Eastern China, China Outflow) due to 100% increase of NO_x in a particular region (China and ROA). The regions of China and ROA (Rest of Asia) are defined in Figure 3. The perturbation values (Pt) are the relative difference between standard and perturbation simulations.

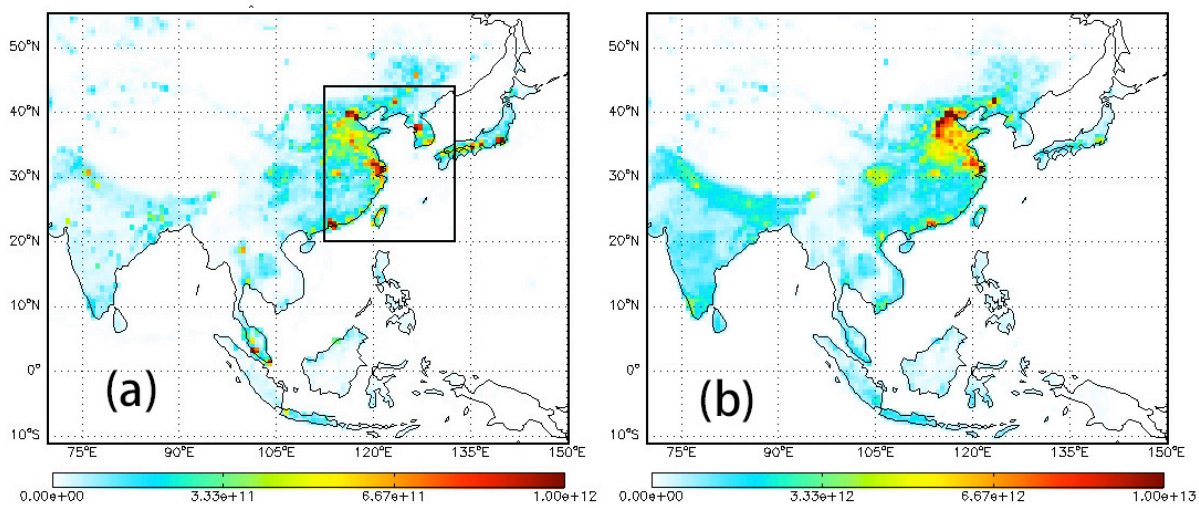

Figure 1. Anthropogenic emission of (a) NO_x and (b) CO in June 2006 as used in GEOS-Chem. The unit is molec/cm^2/s. The black box defines the domains studied in this work. The "East China" domain includes the grids of Chinese mainland within the black box. The "China Outflow region" are grids within the black box, excluding the Chinese mainland.

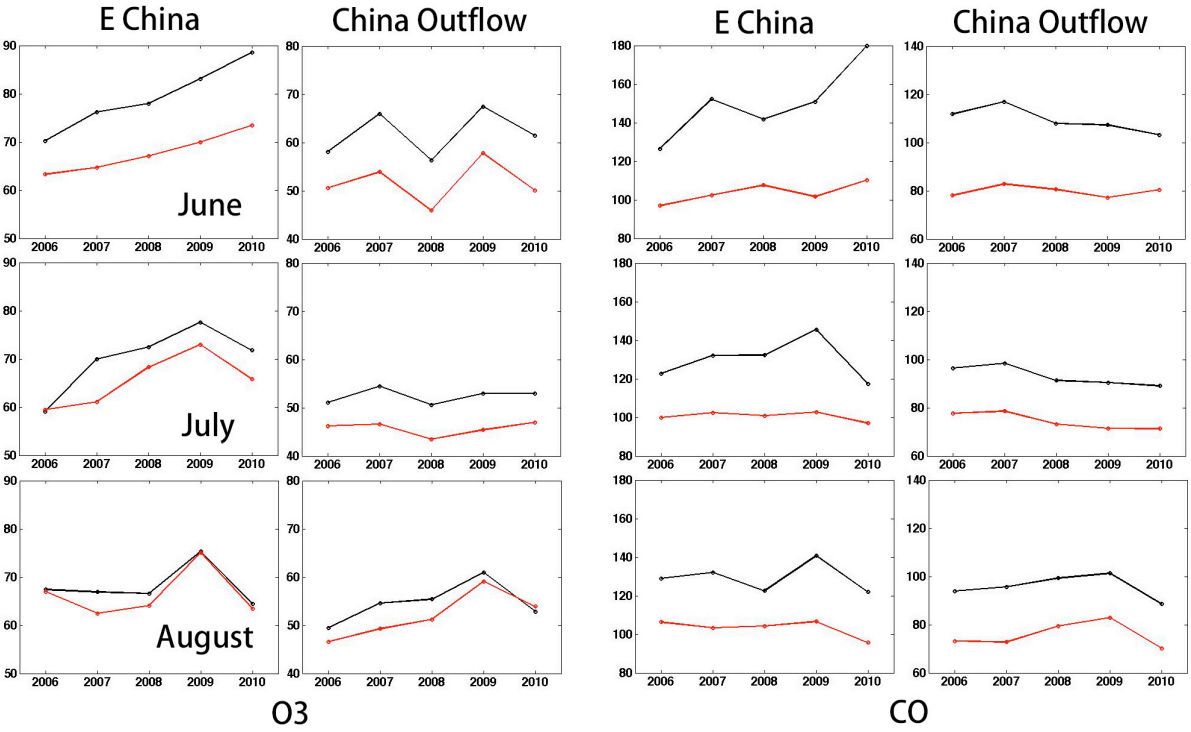

Figure 2. Monthly regional mean O_3 and CO concentration at free troposphere (681 - 383 hPa) in June, July and August 2006-2010. Red line is GEOS-Chem model simulation with a priori emission inventories and black line is TES measurements. The model results are smoothed wth the TES averaging kernels. The TES ozone data are biased high by 7 ppbv.

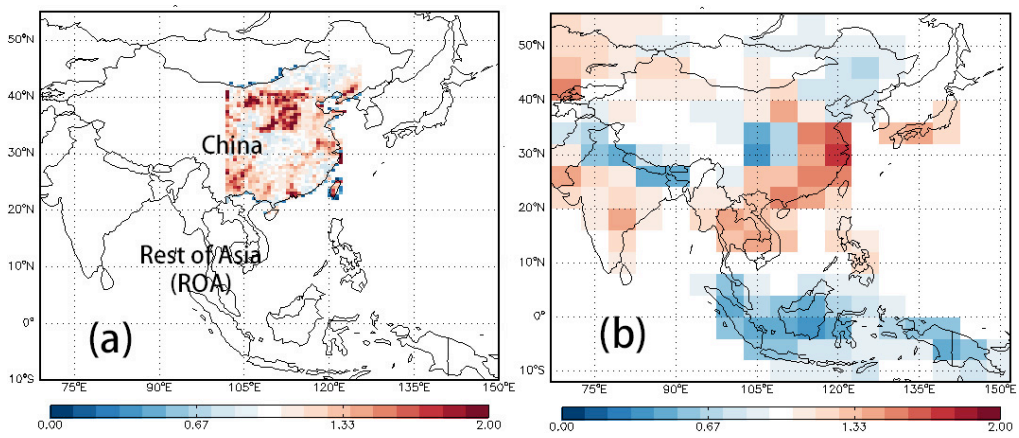

Figure 3. (a) Scaling factors of anthropogenic NO_x for June 2006. (b) Scaling factor of total CO emission (combustion + oxidation from biogenic VOCs) for June 2006.

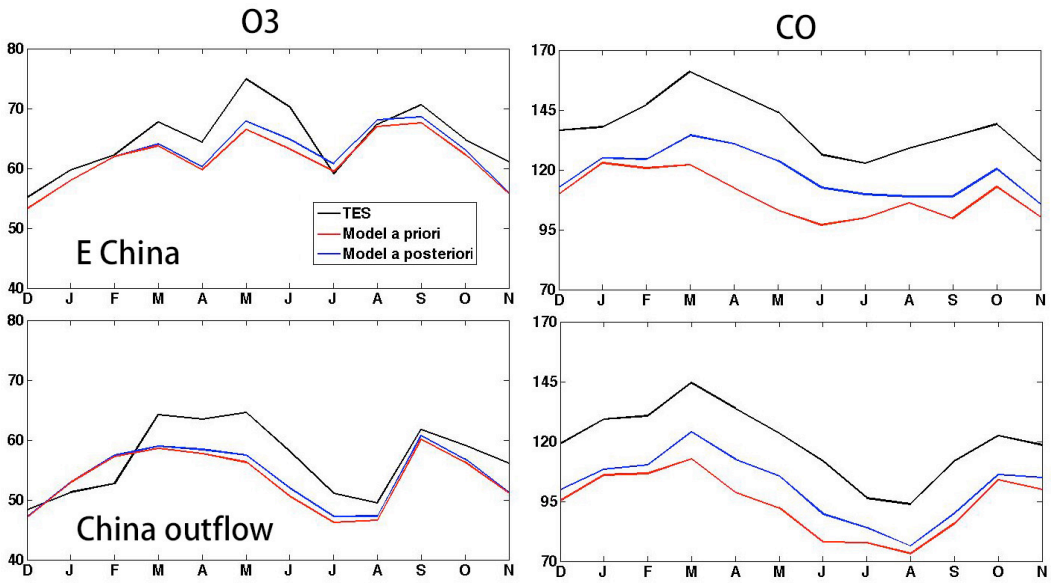

Figure 4. Monthly regional mean O_3 and CO concentration at free troposphere (681 - 383 hPa) in the period of Dec 2005 – Nov 2006. Red line is GEOS-Chem model simulation with a priori emission inventories. Blue line is model simulation with updated NO_x and CO emission inventories. Black line is TES measurements. The model results are smoothed wth the TES averaging kernels. The positive bias in the TES O_3 data is larger in summer and smaller in winter.

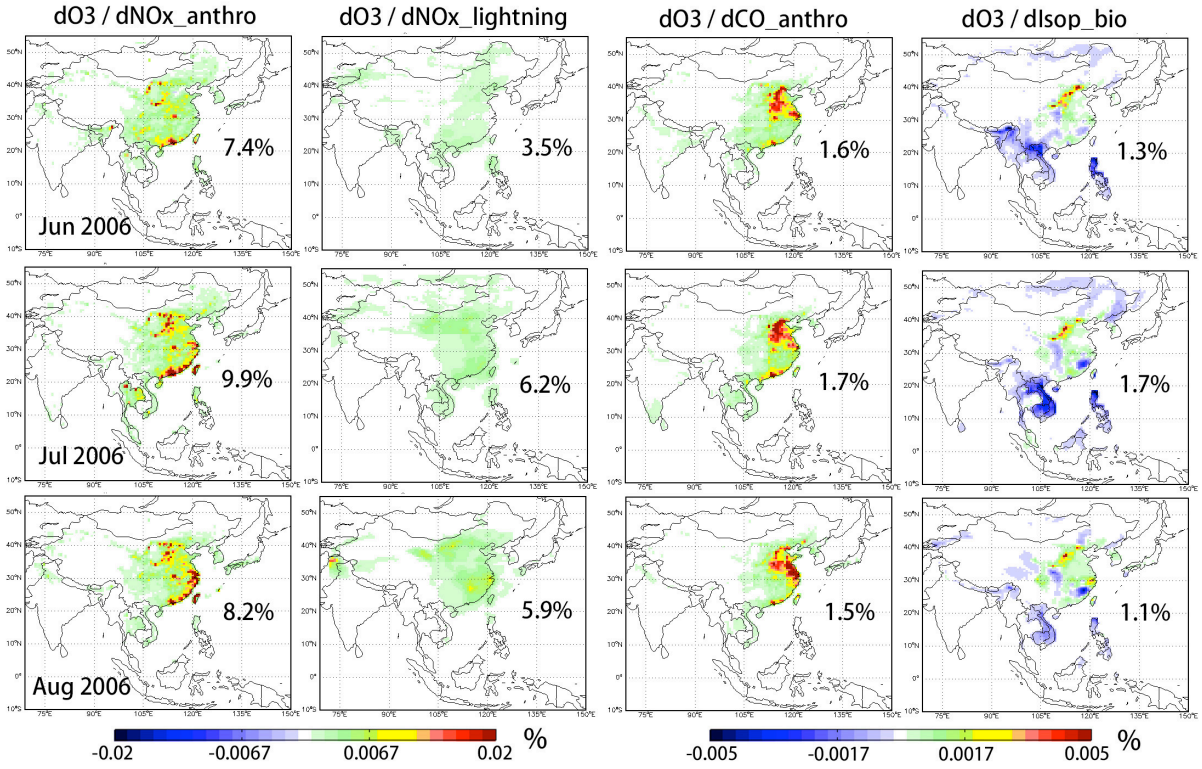

Figure 5. Contributions of anthropogenic NO_x, lightning NO_x, anthropogenic CO, biogenic isoprene on free tropospheric (819 - 396 hPa) O_3 over eastern China derived from the adjoint of GEOS-Chem in June, July and August 2006. The contributions can be explained as the percentage change of regional mean ozone due to a fractional change in the emissions in a particular grid assuming unchanged chemical environment. The numbers are the total of absolute value of pre-cursor contributions for the whole domain shown in the figures.

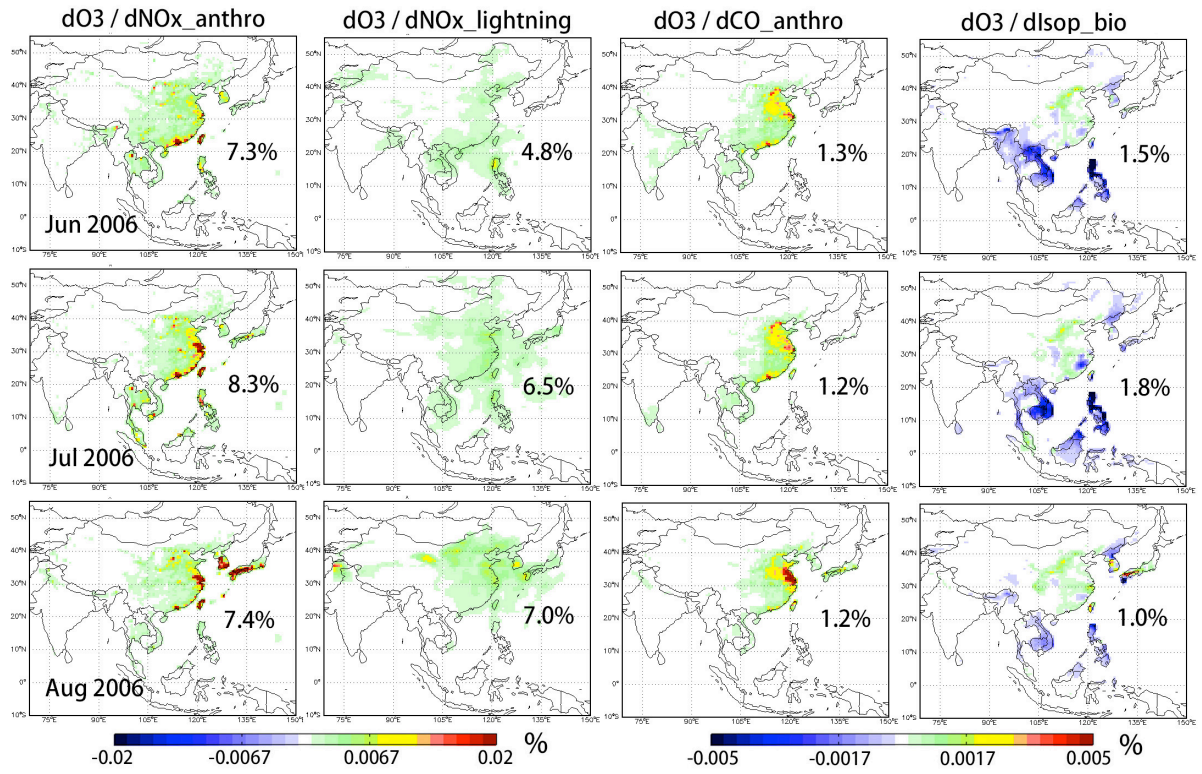

Figure 6. Contributions of anthropogenic NOx, lightning NOx, anthropogenic CO, biogenic isoprene on free tropospheric (819 - 396 hPa) O_3 over China Outflow region derived from the adjoint of GEOS-Chem in June, July and August 2006.

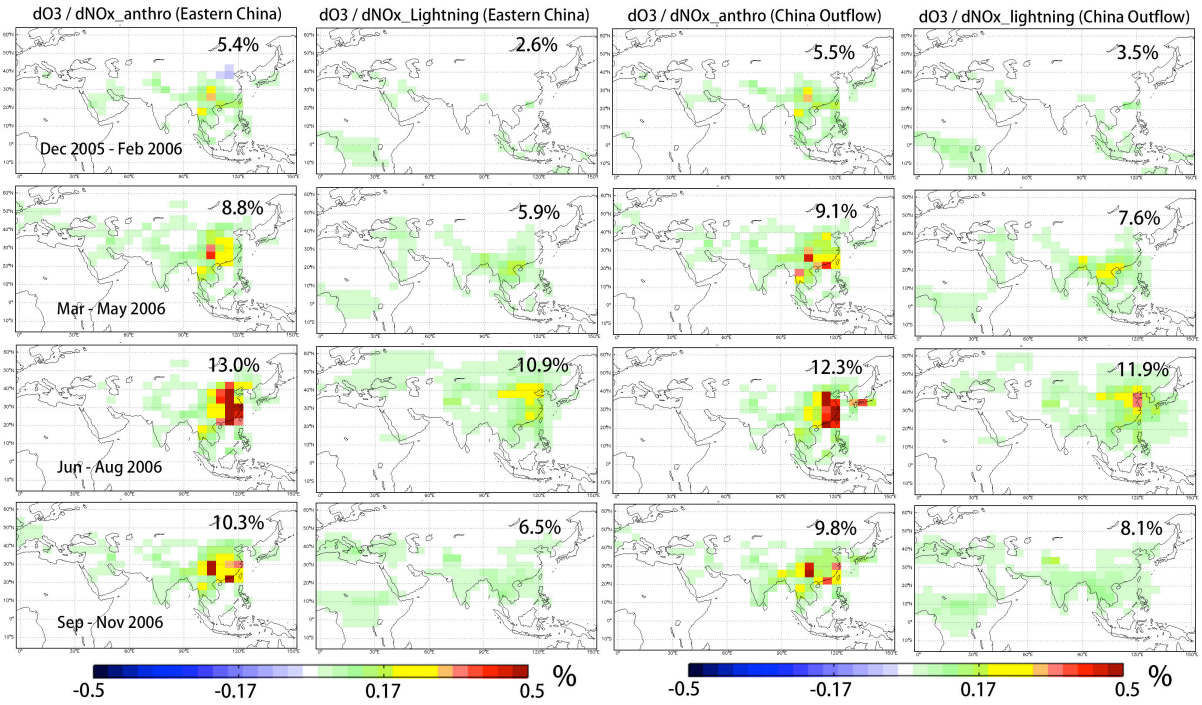

Figure 7. Contributions of anthropogenic NO_x and lightning NO_x on free tropospheric (819 - 396 hPa) O_3 over eastern China and China outflow region in December 2005 – November 2006.